Electronic Supplementary Material (ESI) for Chemical Science.

Supporting Information for

Accessing Metal-Specific Orbital Interactions in C-H Activation with Resonant Inelastic X-ray Scattering

Ambar Banerjee*, Raphael M. Jay* Torsten Leitner, Ru-Pan Wang, Jessica Harich, Robert Stefanuik, Michael R. Coates, Emma V. Beale, Victoria Kabanova, Abdullah Kahraman, Anna Wach, Dmitry Ozerov, Christopher Arrell, Christopher Milne, Philip J. M. Johnson, Claudio Cirelli[4], Camila Bacellar, Nils Huse, Michael Odelius*, Philippe Wernet*

Email: ambar.banerjee@physics.uu.se , raphael.jay@physics.uu.se , odelius@fysik.su.se , philippe.wernet@physics.uu.se

This PDF file includes:

Figures S1 to S8

Comparison of RIXS spectra simulated at the TDDFT and RASPT2 level of theory.

Coordinates for the intermediates, $CpRh(CO)_2$, CpRhCO, CpRhCO-oct, CpRhCO-R-H, $Rh(acac)(CO)_2$ and Rh(acac)CO-oct in Å.

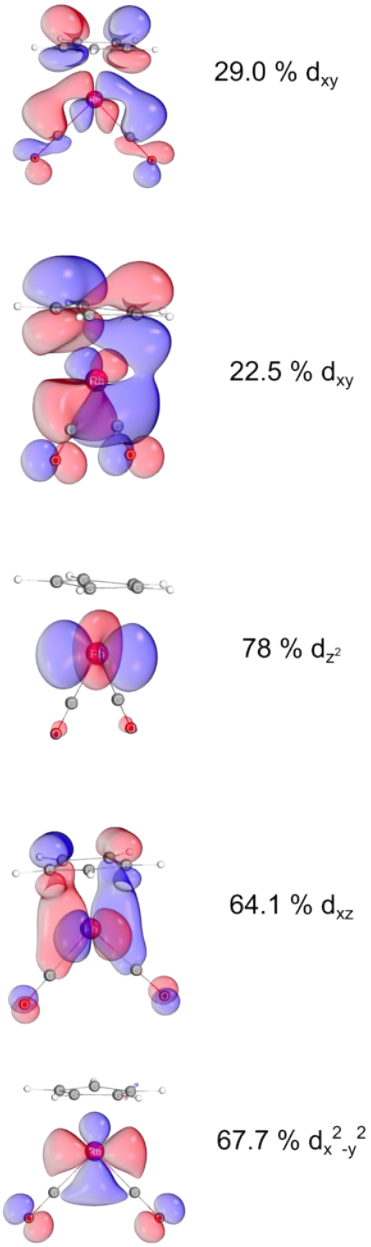

Fig. S1. The frontier molecular (Kohn-Sham) orbitals for $CpRh(CO)_2$ obtained using the B3LYP functional. The 4d characters are additionally given along with the label of each orbital.

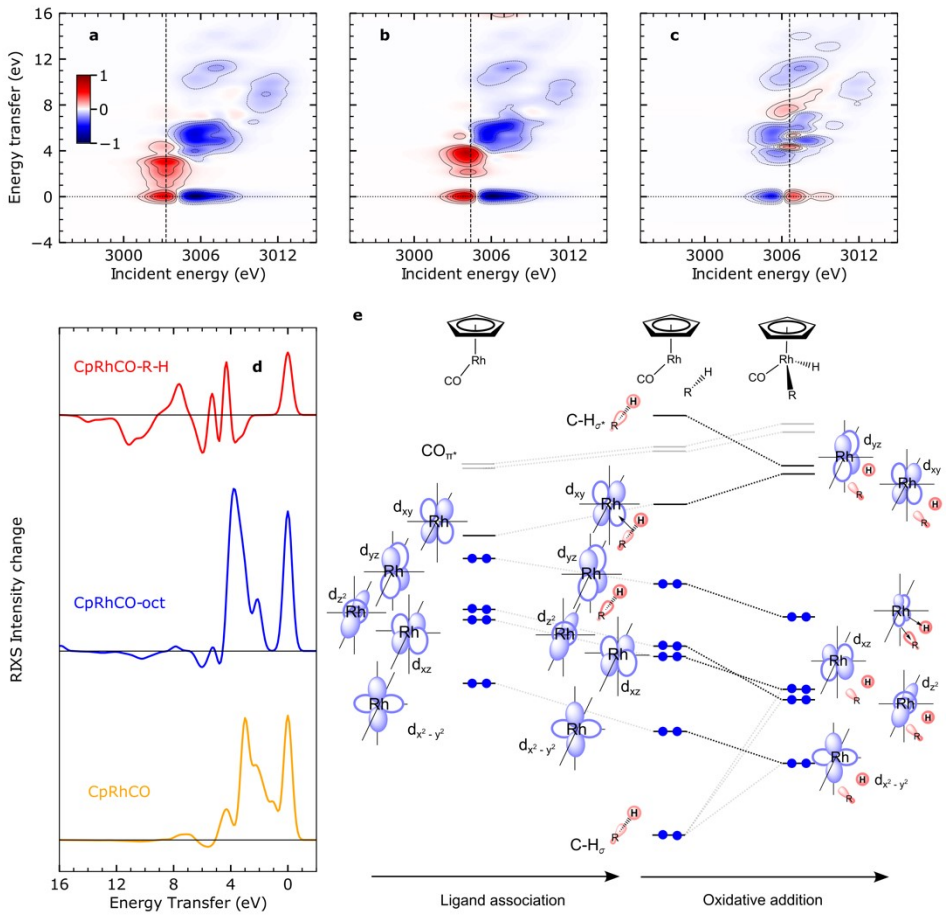

Fig. S2. VtC-RIXS difference maps and spectra for the photoinduced C-H activation by $CpRh(CO)_2$ and the emerging orbital correlation diagram. (a), (b) and (c) show the RIXS difference maps for CpRhCO, CpRhCO-octane and CpRhCO-R-H respectively, obtained by subtracting the RIXS map of $CpRh(CO)_2$ shown in Figure 3 (a) from the RIXS maps shown in Figure 3 (b), (c) and (d) in the main text. The red regions show positive intensity and blue regions show depletion. The vertical lines indicate the incidence energies where cuts were obtained. In panel (c) we show cuts in the difference RIXS maps for CpRhCO in orange, CpRhCO-oct in red and CpRhCO-R-H in blue. Panel (d) shows the correlation diagram, which is derived from interpreting the RIXS spectra for CpRhCO, CpRhCO-octane and CpRhCO-R-H as shown in panel (c). The dotted black lines connecting the four occupied 4d orbitals in this panel deduced from the grey connecting lines in panel (c).

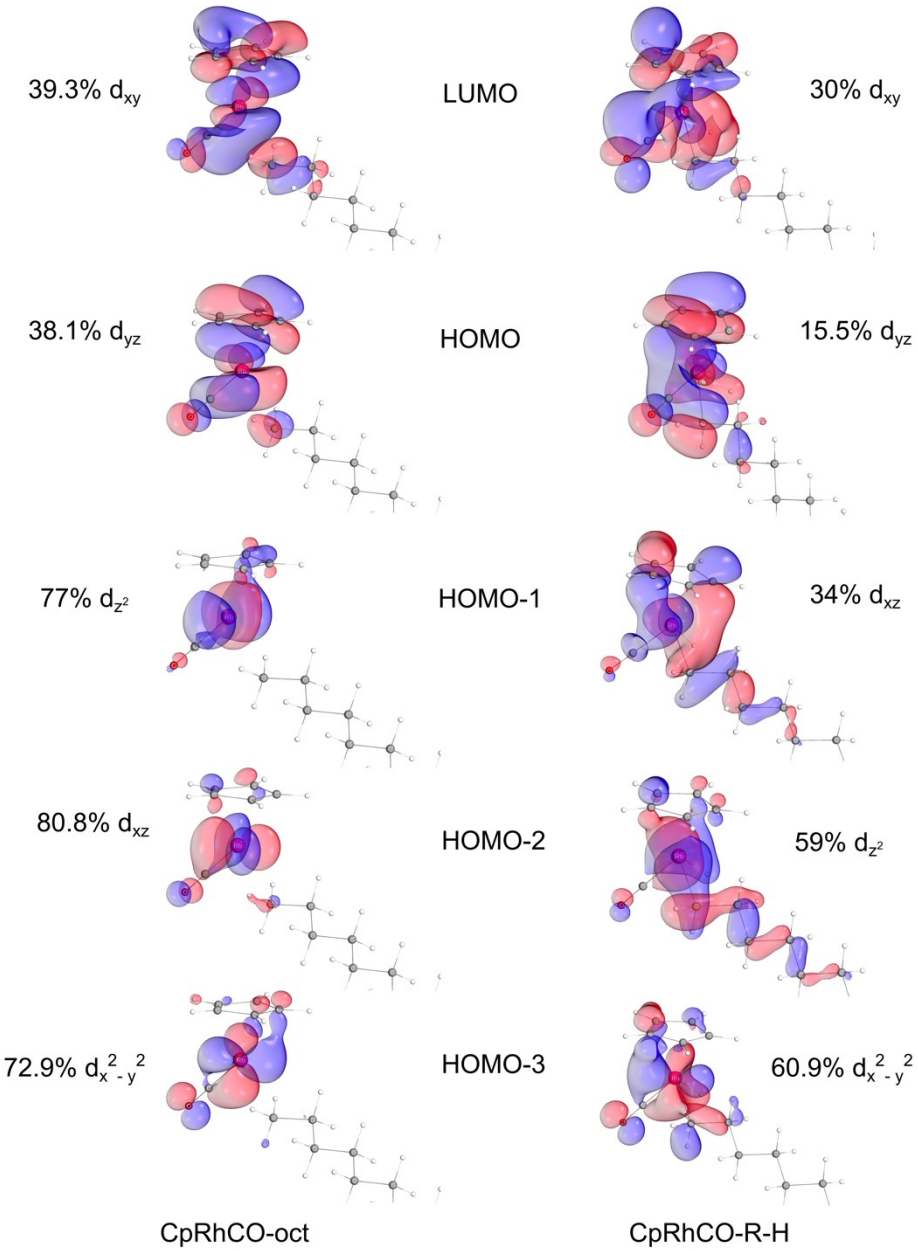

Fig. S3: The frontier molecular (Kohn-Sham) orbitals for CpRhCO-octane and CpRhCO-R-H obtained using the B3LYP functional. The 4d characters are additionally given along with the label of each orbital.

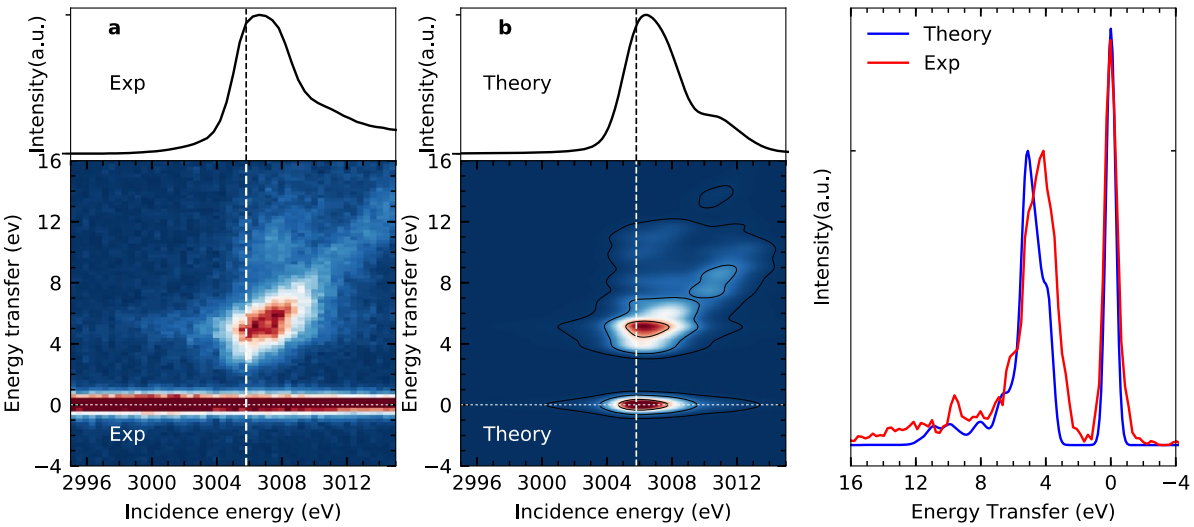

Fig. S4: **VtC-RIXS intensities (maps) for Rhacac(CO)$_2$ and cuts at a specific incidence energy to target the MC d-d final states.** (a) Experimental X-ray absorption spectrum (top) and RIXS map (bottom) for Rh(acac)(CO)$_2$. (b) Simulated X-ray absorption spectrum and RIXS map at the TD-DFT level of theory (vertical dashed lines in (a) and (b) indicate the energy of 3005.8 eV at which cuts were obtained to target the MC d-d states). (c) Cuts from the experimental and simulated RIXS maps at 3005.8 eV, where individual peaks correspond to different 4d (occupied) → 4d (LUMO) orbital transitions (transitions from the ground to MC valence-excited states).

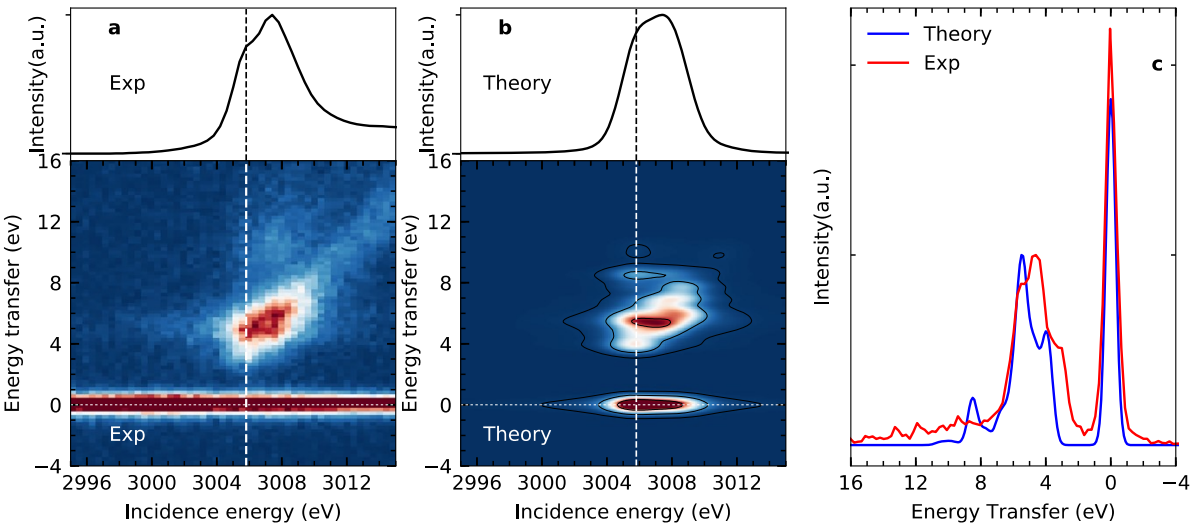

Fig. S5: The VtC-RIXS map for $CpRh(CO)_2$ at the RASPT2 level of theory. (a) Experimental X-ray absorption spectrum (top) and RIXS map (bottom) for $CpRh(CO)_2$. (b) Simulated X-ray absorption spectrum and RIXS map at the RASPT2 level of theory (vertical dashed lines in (a) and (b) indicate the energy of 3005.8 eV at which cuts were obtained to target the MC d-d states). (c) Cuts from the experimental and simulated RIXS maps at 3005.8 eV where individual peaks correspond to different 4d (occupied) → 4d (LUMO) orbital transitions (transitions from the ground to MC valence-excited states).

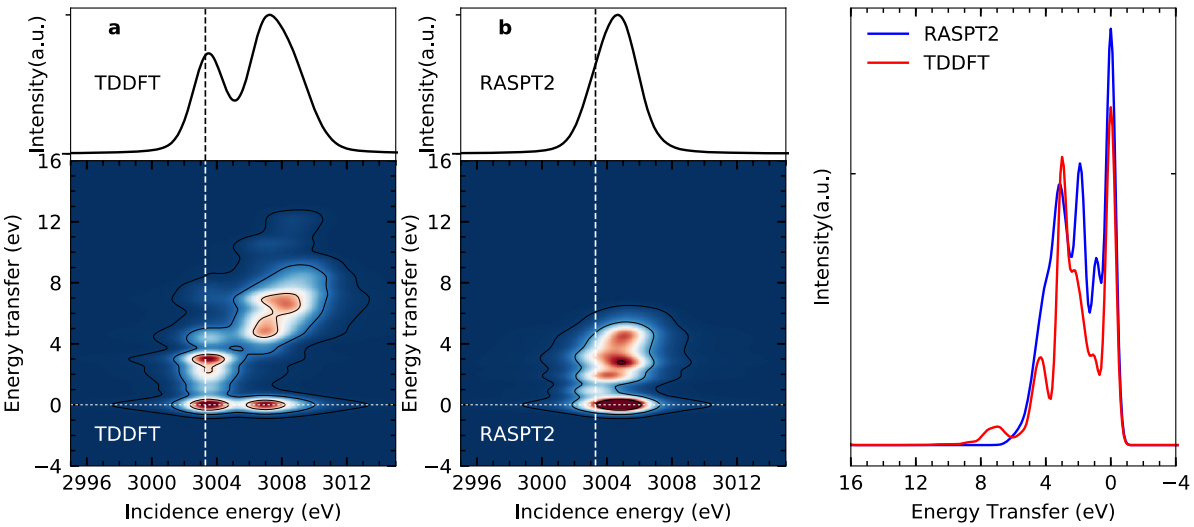

Fig. S6: Comparison of simulated VtC-RIXS map for CpRh(CO) at the RASPT2 and TD-DFT level of theory. (a) Simulated X-ray absorption spectrum and RIXS map at the TD-DFT level of theory (b) Simulated X-ray absorption spectrum and RIXS map at the RASPT2 level of theory (vertical dashed lines in (a) and (b) indicate the energy of 3003.3 eV at which cuts were obtained to target the MC d-d states). (c) Cuts from the experimental and simulated RIXS maps at 3003.3 eV where individual peaks correspond to different 4d (occupied) → 4d (LUMO) orbital transitions (transitions from the ground to MC valence-excited states).

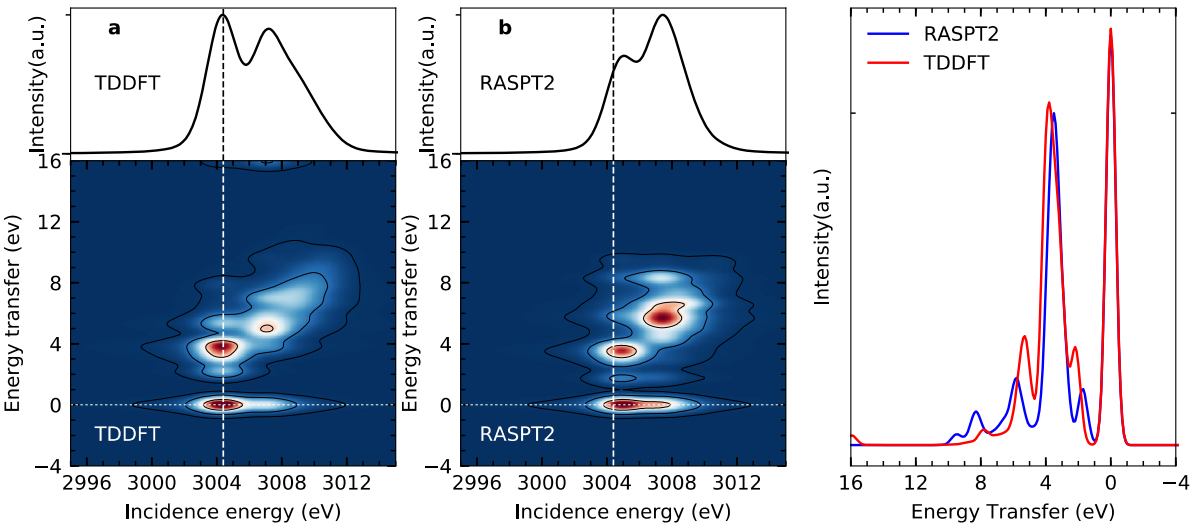

Fig. S7: Comparison of simulated VtC-RIXS map for CpRhCO-octane at the RASPT2 and TD-DFT level of theory. (a) Simulated X-ray absorption spectrum and RIXS map at the TD-DFT level of theory (b) Simulated X-ray absorption spectrum and RIXS map at the RASPT2 level of theory (vertical dashed lines in (a) and (b) indicate the energy of 3004.4 eV at which cuts were obtained to target the MC d-d states). (c) Cuts from the experimental and simulated RIXS maps at 3004.4 eV where individual peaks correspond to different 4d (occupied) → 4d (LUMO) orbital transitions (transitions from the ground to MC valence-excited states).

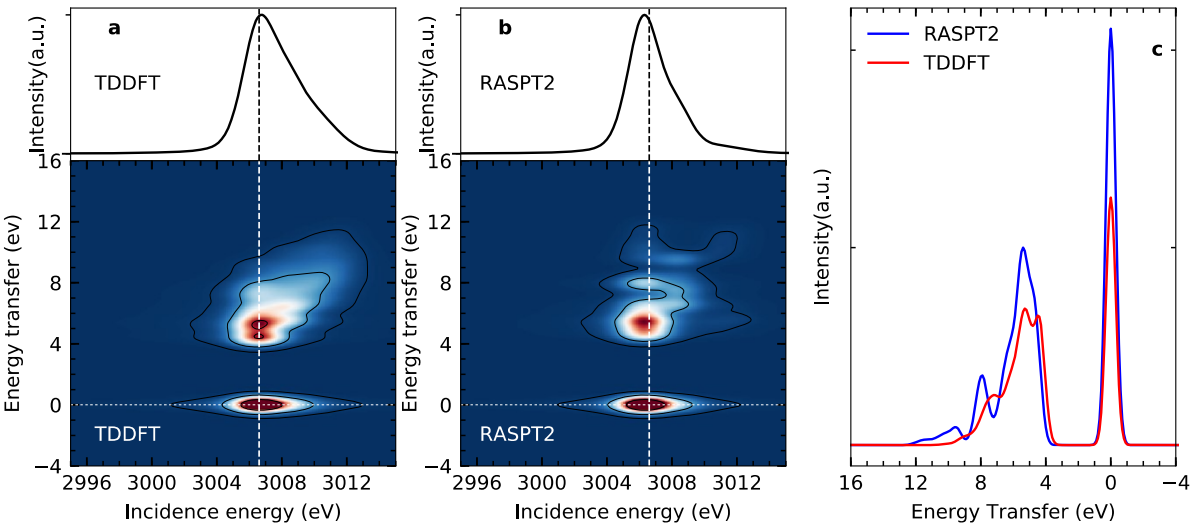

Fig. S8: Comparison of simulated VtC-RIXS map for CpRhCO-R-H at the RASPT2 and TD-DFT level of theory. (a) Simulated X-ray absorption spectrum and RIXS map at the TD-DFT level of theory (b) Simulated X-ray absorption spectrum and RIXS map at the RASPT2 level of theory (vertical dashed lines in (a) and (b) indicate the energy of 3006.6 eV at which cuts were obtained to target the MC d-d states). (c) Cuts from the experimental and simulated RIXS maps at 3006.6 eV where individual peaks correspond to different 4d (occupied) → 4d (LUMO) orbital transitions (transitions from the ground to MC valence-excited states).

Comparison of RIXS spectra simulated at the TDDFT and RASPT2 level of theory.

As shown in Figure S5, X-ray absorption and RIXS spectra for $CpRh(CO)_2$ simulated at the RASPT2 level of theory reproduce the experimentally measured spectra. The agreement, however, is not as good as with that with the spectra simulated at the TDDFT level of theory. For the X-ray absorption spectra, the relative intensity of the pre-edge and the main peak is not correctly reproduced at the RASPT2 level of theory. However, for the RIXS spectra, RASPT2 simulations captures all the features but the energetic splittings are lower and the relative intensities are also not well reproduced. Thus, we can safely conclude that restricted subspace TDDFT indeed performs better than RASPT2, in reproducing the steady state RIXS spectra of $CpRh(CO)_2$, as also demonstrated earlier[1,2]. One could expect that for the low valent CpRhCO complex, and hence being multireference, RASPT2 will do a better job than TDDFT. However, in Figure S6 we see that, although the pre-edge for the X-ray absorption spectra, is captured, the main peak is missing from the spectra at the RASPT2 level of theory. This could be due to limited number of roots solved in the RASSCF/RASPT2 calculations. For the cut in RIXS map at the pre-edge peak, as shown in Figure S6(c), RASPT2 captures all the relevant peaks and is energetically comparable to the TDDFT spectra, but with different relative intensities. RASPT2 in agreement with TDDFT reproduces the red shifting of the lowest energy RIXS peak to less than 1eV energy loss and merges with the elastic line. For CpRhCO-oct, as shown in Figure S7, the agreement between TDDFT and RASPT2 is much better. RASPT2 captures the blue shifting of the lowest energy RIXS peak from less that 1eV to about 1.8 eV, as compared to 2eV predicted by TDDFT. Here too, the relative intensities differ between TDDFT and RASPT2. Lastly, in the case of CpRhCO-C-H, see Figure S8, RASPT2 captures the further blue shifting of the lowest energy RIXS peaks and the merging with other RIXS feature as also predicted by TDDFT, with disagreements remaining in the peak intensities and energetic splittings. Thus, a qualitative agreement between RASPT2 and TDDFT can be observed, and broadly the same conclusions, as drawn from the TDDFT simulations, can also be drawn from RASPT2 calculations.

Coordinates for the intermediates, $CpRh(CO)_2$, CpRhCO, CpRhCO-oct, CpRhCO-R-H, $Rh(acac)(CO)_2$ and Rh(acac)CO-oct in Å.

$CpRh(CO)_2$

Rh	-1.159571	0.139492	-0.338052
C	0.819406	0.354179	-1.488742
C	-1.533074	0.589617	1.428926
C	-0.152947	-0.299172	-2.295219
C	1.012988	-0.459629	-0.343042
C	-0.459101	-1.580564	-1.709412
C	0.253068	-1.676513	-0.504345
C	-2.797494	0.872023	-0.826926
H	1.276300	1.310904	-1.683386
H	-0.539404	0.065274	-3.235039
H	1.673598	-0.241461	0.482890
H	-1.136000	-2.315762	-2.115853
H	0.228579	-2.500529	0.192148
O	-1.768176	0.876069	2.517320
O	-3.807898	1.331281	-1.127469

CpRhCO

Rh	-0.702876	0.405724	-0.353738
C	1.394001	-0.135847	-1.023414
C	0.304797	-0.732253	-1.782313
C	1.283097	-0.633108	0.277271
C	-0.335768	-1.746164	-0.957965
C	0.220031	-1.622909	0.317441
C	-1.774816	1.504552	-1.363038
H	2.109503	0.583186	-1.388613
H	0.126058	-0.583203	-2.837128
H	1.889975	-0.342039	1.122772
H	-1.118284	-2.420348	-1.267196
H	-0.079090	-2.175155	1.196750
O	-2.460036	2.204116	-1.980491

CpRhCO-oct

Rh	-0.364515	-0.997671	-4.174590
C	1.749692	-1.506943	-4.907682
C	0.676434	-2.134151	-5.649916
C	1.663644	-1.986717	-3.597018
C	0.058329	-3.137182	-4.810831
C	0.616644	-2.989637	-3.534166
C	-1.448693	0.075819	-5.195290
H	2.440216	-0.769879	-5.285481
H	0.484797	-1.999157	-6.704271
H	2.278149	-1.675755	-2.764223
H	-0.720575	-3.822935	-5.103915
H	0.337545	-3.544336	-2.650223

O	-2.134068	0.750683	-5.839627
C	-0.521705	0.797732	0.386802
H	0.441109	1.234721	0.094718
C	-0.888946	-0.312244	-0.602662
H	-0.133618	-1.104358	-0.562748
H	-1.837322	-0.772285	-0.303556
H	-1.258161	1.607002	0.308982
C	-1.002273	0.220288	-2.032580
H	-1.764849	0.995059	-2.124796
H	-0.056879	0.646714	-2.374546
H	-1.412269	-0.632939	-2.682180
C	0.057790	1.003256	4.264114
H	-0.910033	0.604322	4.592067
H	0.771466	0.173502	4.342804
C	-0.041362	1.448948	2.804189
H	-0.764454	2.270222	2.724338
H	0.924077	1.863980	2.489324
C	-0.442332	0.328579	1.841301
H	0.279690	-0.493581	1.921113
H	-1.411582	-0.085509	2.144524
C	0.489116	2.127985	5.208548
H	-0.237921	2.946413	5.150125
H	1.442356	2.542054	4.860033
C	0.632326	1.672515	6.660891
H	-0.313702	1.280785	7.046126
H	1.379254	0.878114	6.751708
H	0.942626	2.496586	7.308595

CpRhCO-R-H

Rh	-0.574792	-0.975947	-3.848177
C	1.476755	-1.604893	-4.744833
C	0.463643	-2.473821	-5.272005
C	1.507130	-1.780078	-3.343571
C	-0.118368	-3.181523	-4.196940
C	0.503221	-2.733038	-2.986679
C	-1.448176	0.265947	-4.884931
H	2.109147	-0.945094	-5.318866
H	0.194125	-2.572348	-6.312803
H	2.154157	-1.257737	-2.655558
H	-0.907195	-3.913755	-4.269579
H	0.297408	-3.101707	-1.994740
O	-2.028711	1.028317	-5.520548
C	-0.371006	0.977431	0.183721
H	0.474052	1.646842	-0.020007
C	-0.431848	-0.106319	-0.905217
H	0.463801	-0.732348	-0.820705
H	-1.285798	-0.763479	-0.710113
H	-1.273067	1.598918	0.128954
C	-0.538892	0.483353	-2.305931
H	-1.427047	1.114066	-2.377510
H	0.330086	1.107201	-2.536682
H	-1.980557	-1.188541	-3.205051
C	0.093506	0.887213	4.086402
H	-0.774235	0.266712	4.343374
H	0.959175	0.212210	4.083878
C	-0.093150	1.468800	2.683135
H	-0.977815	2.117814	2.671742
H	0.761190	2.115450	2.446718
C	-0.228836	0.401170	1.595148

H	0.650368	-0.255473	1.627936
H	-1.092919	-0.237924	1.815541
C	0.293307	1.952352	5.166927
H	-0.579634	2.615352	5.187114
H	1.148526	2.582090	4.894566
C	0.519087	1.362365	6.559830
H	-0.336250	0.756769	6.874248
H	1.402694	0.716858	6.574775
H	0.666916	2.146796	7.306435

$Rh(acac)(CO)_2$

C	0.229078	0.382875	2.581407
C	0.207386	-2.231504	2.495667
O	0.241314	1.167976	3.415150
O	0.207136	-3.085351	3.258672
C	0.241108	-0.807558	-2.119091
Rh	0.212076	-0.881998	1.227199
O	0.224029	0.584840	-0.182053
C	0.238953	0.421387	-1.450118
C	0.214859	-2.063801	-1.504772
O	0.196905	-2.281718	-0.245087
H	0.258501	-0.784113	-3.201157
C	0.191037	-3.309553	-2.352666
C	0.239534	1.701032	-2.247362
H	0.423522	1.522191	-3.306740
H	0.997171	2.379541	-1.851030
H	-0.730760	2.193819	-2.133758
H	0.368679	-3.091656	-3.405649
H	-0.784801	-3.793322	-2.248807
H	0.942666	-4.012912	-1.989548

Rh(acac)CO-oct

C	-0.629227	-1.543461	-1.375037
O	-0.169637	0.347202	-0.005383
C	-0.731328	-0.194914	-1.020079
C	0.099781	-2.522126	-0.687376
O	0.784765	-2.355441	0.380276
H	-1.158395	-1.861899	-2.263013
C	0.117631	-3.937354	-1.206533
C	-1.553967	0.740267	-1.866179
H	-2.024033	0.225340	-2.702943
H	-0.914852	1.541280	-2.247234
H	-2.324674	1.205021	-1.245856
H	-0.474724	-4.042303	-2.114451
H	-0.273168	-4.609539	-0.438433
H	1.148892	-4.236896	-1.409291
C	1.984842	-1.433512	2.633712
O	2.627221	-1.943111	3.444691
Rh	0.964031	-0.620809	1.354818
C	2.760304	3.365698	3.408355
H	3.576586	3.172620	2.701583
C	1.929202	2.091886	3.578706
H	2.555516	1.298585	3.997998
H	1.127273	2.273893	4.302152
H	2.136719	4.146013	2.954947
C	1.324815	1.621880	2.255967

H	0.662573	2.359097	1.799414
H	2.110204	1.383252	1.528709
H	0.619310	0.757581	2.515784
C	4.724712	5.696740	5.881389
H	3.897981	5.883135	6.578605
H	5.351152	4.925937	6.347822
C	4.162157	5.162667	4.562812
H	3.538470	5.935874	4.096769
H	4.988857	4.974134	3.866477
C	3.338900	3.883785	4.726704
H	3.964607	3.104716	5.179226
H	2.519370	4.068877	5.432264
C	6.093723	7.510812	7.041259
H	6.746014	6.774439	7.520231
H	5.283937	7.742403	7.739700
C	5.543475	6.978816	5.718143
H	4.919106	7.746692	5.246395
H	6.373276	6.790557	5.026805
H	6.675709	8.424009	6.891245

References

1 E. Biasin, D. R. Nascimento, B. I. Poulter, B. Abraham, K. Kunnus, A. T. Garcia-Esparza, S. H. Nowak, T. Kroll, R. W. Schoenlein, R. Alonso-Mori, M. Khalil, N. Govind and D. Sokaras, *Chem. Sci.*, 2021, **12**, 3713–3725.

2 D. R. Nascimento, E. Biasin, B. I. Poulter, M. Khalil, D. Sokaras and N. Govind, *J. Chem. Theory Comput.*, 2021, **17**, 3031–3038.